CrossMark

INVITED PAPER

Stabilizing new bismuth compounds in thin film form

Aiping Chen[a)]
Center for Integrated Nanotechnologies (CINT), Los Alamos National Laboratory, Los Alamos, New Mexico 87545, USA

Honghui Zhou
Department of Materials Science and Engineering, NSF Center for Advanced Materials and Smart Structures, North Carolina State University, Raleigh, North Carolina 27695, USA

Yuanyuan Zhu
Physical & Computational Sciences Directorate, Pacific Northwest National Laboratory, Richland, Washington 99352, USA

Leigang Li and Wenrui Zhang
Department of Electrical and Computer Engineering, Texas A&M University, College Station, TX 77843, USA

Jagdish Narayan
Department of Materials Science and Engineering, NSF Center for Advanced Materials and Smart Structures, North Carolina State University, Raleigh, North Carolina 27695, USA

Haiyan Wang
Department of Electrical and Computer Engineering, Texas A&M University, College Station, TX 77843, USA; and School of Materials Engineering, Electrical and Computer Engineering, Purdue University, West Lafayette, IN 47907, USA

Quanxi Jia[b)]
Center for Integrated Nanotechnologies (CINT), Los Alamos National Laboratory, Los Alamos, New Mexico 87545, USA

(Received 6 June 2016; accepted 6 October 2016)

Growth of unexpected phases from a composite target of $BiFeO_3$:$BiMnO_3$ and/or $BiFeO_3$:$BiCrO_3$ has been explored using pulsed laser deposition. The Bi_2FeMnO_6 tetragonal phase can be grown directly on $SrTiO_3$ (STO) substrate, while two phases (S1 and S2) were found to grow on $LaAlO_3$ (LAO) substrates with narrow growth windows. However, introducing a thin CeO_2 buffer layer effectively broadens the growth window for the pure S1 phase, regardless of the substrate. Moreover, we discovered two new phases (X1 and X2) when growing on STO substrates using a $BiFeO_3$:$BiCrO_3$ target. Pure X2 phase can be obtained on CeO_2-buffered STO and LAO substrates. This work demonstrates that some unexpected phases can be stabilized in a thin film form by using composite perovskite $BiRO_3$ (R = Cr, Mn, Fe, Co, Ni) targets. Furthermore, it also indicates that CeO_2 can serve as a general template for the growth of bismuth compounds with potential room-temperature multiferroicity.

I. INTRODUCTION

The synthesis of complex oxides with multiple transition metals has attracted much attention in the past decades as these materials could exhibit emergent properties. Recent advances in controlled growth of thin films have provided unique opportunities to grow novel complex oxides, which are inaccessible in bulk process. Pulsed laser deposition (PLD) is a relatively simple and very versatile technique for thin film growth.[1] Different architectures including heterostructures,[2–4] superlattices,[5–7] and vertical heteroepitaxial nanocomposites,[8–10] have been reported. Recent efforts on vertical heteroepitaxial nanocomposites have been focused on the development of multifunctionalities by combining two immiscible phases.[11–17] Immiscibility is one of the key factors for nanocomposite formation.[18] On the other hand, the co-growth of two miscible or partially miscible phases can lead to unexpected phases.[19–21] A representative system is ferroelectric $BiFeO_3$ (BFO) in combination with ferromagnetic $BiMnO_3$ (BMO) where double perovskites can be produced to achieve ferromagnetism and multiferroicity.[22–26] For example, Chio et al. reported room temperature multiferroic properties in strained $BiFe_{0.5}Mn_{0.5}O_3$ thin films,[27] and increased ferromagnetic Curie temperature in BFO/BMO superlattices.[28] Similarly, other materials

Contributing Editor: Ian M. Reaney
Address all correspondence to these authors.
[a)]e-mail: apchen@lanl.gov
[b)]e-mail: qxjia@lanl.gov
DOI: 10.1557/jmr.2016.391

 © Materials Research Society 2016

https://doi.org/10.1557/jmr.2016.391 Published online by Cambridge University Press

with double perovskite structure such as Bi_2NiMnO_6 and Bi_2FeCrO_6 can be synthesized using the same scheme.[29–32]

The microstructure (and thus the functionality) of a given material grown by PLD is influenced by many factors including substrate, gas pressure, temperature, laser frequency, and laser energy density. Substrate plays a critical role in epitaxial growth of thin film as the lattice mismatch between the film and the substrate determines the critical thickness. More importantly, substrate can be used to stabilize the phase if multiple phases co-exist for a given chemical composition. For example, $LaAlO_3$ substrate was used to stabilize the anatase TiO_2 phase while r- and m-sapphire substrates were selected for the growth of rutile TiO_2 phase.[33,34] VO_2 (B) phase was found prone to grown on $SrTiO_3$ substrate, whereas, VO_2 (M) phase often found grown on c-sapphire by domain matching epitaxy.[35–38] Oxygen pressure during film growth is usually associated to the oxygen content in the metal oxide films.[39] Another important but often ignored effect induced by oxygen pressure is cation stoichiometry,[3,5,40–42] which is one of the key factors determining functional properties.[43] In the case of growth temperature, it not only influences the film crystallinity and feature size, but also affects the phase structure.[44] Regarding materials with high volatility such as bismuth, vanadium, and lithium, lower growth temperature below 700 °C is usually used.[45–47] Laser repetition rate is found to alter the material structure. For example, it was reported that 5 Hz repetition rate results in VO_2 (A) phase while 2 Hz results in VO_2 (B) phase.[45] In vertical nanocomposites, laser repetition rate can affect the feature size.[48] The laser energy density of the excimer lasers for the growth of metal oxide films typically ranges from 1 to 3 J/cm^2. Laser energy density is often found to affect cation stoichiometry.[40,41,49,50] Hence, it is critical to maintain a uniform and stable laser energy density to reproducibly grow high quality films.[51]

Bismuth compounds have different structures and are sensitive to growth conditions and substrate.[42,46] Hence, studying the growth window for new phases in thin film form is critical. Alternatively, it is equally important to develop new and versatile strategies to broaden the growth window for desired thin film materials. In this work, we explored the growth of different phases of materials by using $BiFeO_3$:$BiMnO_3$ and $BiFeO_3$:$BiCrO_3$ composite systems. By varying the substrate, deposition temperature, laser repetition rate, and oxygen pressure, we have found the growth of several new phases which have not been reported in the literature. More importantly, we found that the CeO_2 buffer layer, serving as a universal template, is capable of broadening the thin film growth window for new phases.

II. EXPERIMENTAL

PLD was used to grow epitaxial films on STO (001) and LAO (001) substrates. Composite targets, with a 1:1 molar ratio of $Bi_{1.05}FeO_3$ and $Bi_{1.05}MnO_3$, were obtained by conventional ceramic sintering process. The substrate temperature ranged from 650 to 725 °C and oxygen pressure of 15–200 mTorr were maintained during depositions. After deposition, films were in situ annealed for 1 h at 400 °C in an oxygen pressure of 300 Torr before cooling down to room temperature at 5 °C/min. Films with thickness from 10 nm to 300 nm were deposited. A set of thin films were deposited by systematically varying the deposition temperature, laser repetition frequency, deposition duration, oxygen pressure, and different buffer layers. Buffer layer CeO_2 with a thickness of 25 nm was deposited at 700 °C between the film and the substrate. The microstructure was examined by X-ray diffraction (XRD; Bruker D8 powder X-ray diffractometer, Bruker Corporation, Karlsruhe, Germany; and PANalytical MRD PRO X-ray

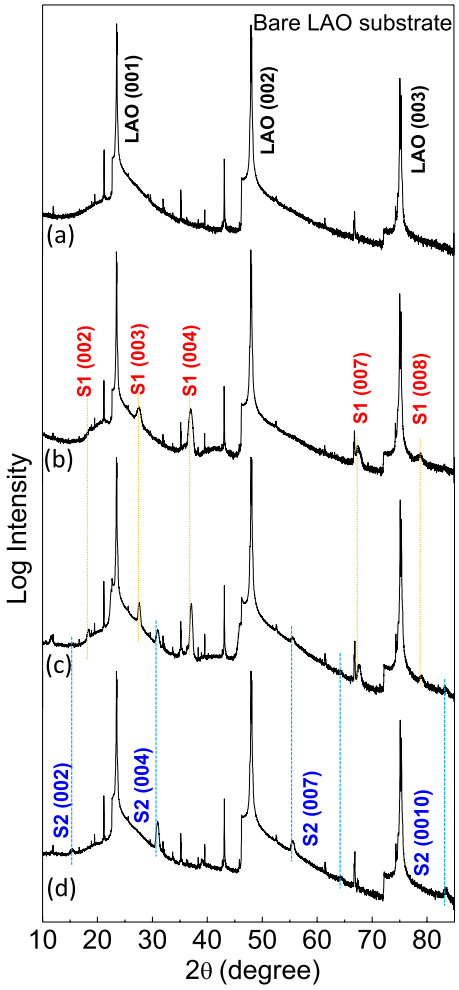


FIG. 1. The XRD patterns of (a) bare LAO substrate, (b) film deposited at 700 °C, 2 Hz, (c) film grown at 700 °C, 4 Hz, (d) film grown at 725 °C and 1 Hz.

https://doi.org/10.1557/jmr.2016.391 Published online by Cambridge University Press

diffractometer, PANalytical, Almelo, The Netherlands) and transmission electron microscopy (TEM; JEOL JEM-2010, JEOL Ltd., Tokyo, Japan; and FEI Tecnai G2 F20, FEI Company, Hillsboro, Oregon). The high-angle annular dark-field scanning transmission electron microscopy (HAADF-STEM) images were taken by using a VG Microscopes HB603U STEM equipped with Nion aberration corrector operating at 300 kV at Oak Ridge National Laboratory (Oak Ridge, Tennessee).

III. RESULTS AND DISCUSSIONS

Figure 1 shows the effect of growth temperature and laser frequency on the films deposited using a BFO:BMO composite target. It can be seen that the phase of films is very sensitive to the growth parameters and the growth window for pure phase is narrow. Figure 1(a) shows a typical XRD θ–2θ scan of a bare LAO substrate from a powder X-ray diffractometer. Figure 1(b) shows the XRD of the film grown at 700 °C and 2 Hz. It can be seen that a single set of diffraction peaks (2θ = 18.28°, 27.57°, 36.96°, ...), can be observed, indicating the growth of a single phase material.[19] This phase is defined as S1 phase. The out-of-plane *d*-spacing of S1 phase is determined to be 4.85 Å. Increasing the laser repetition rate above 4 Hz and tuning the growth temperature either below 670 °C or above 700 °C, as shown in Fig. 1(c), result in mixed phases. Interestingly, when keeping the growth temperature at 725 °C and laser repetition rate at 1 Hz, the film shows a single set of diffraction peaks (2θ = 15.42°, 30.96°, 39.03°, ...), indicating the growth of another pure phase (labeled as S2 phase). The out-of-plane *d*-spacing of S2 phase is determined to be 5.74 Å. The cation ratio for S1 phase is Bi:Fe:Mn = 3:2:2. We expect there are less Bi in S2 phase as it was grown at higher growth temperature and lower laser repetition rate. Thus, the thin film growth in BFO:BMO system is sensitive to the growth condition. The sensitivity of the growth likely stems from the volatilization of the bismuth at different growth conditions.

To study the microstructure of these materials, high resolution STEM has been used. Figure 2(a) shows a typical cross-sectional HAADF-STEM image for S1 phase grown on LAO (001) substrate. Interestingly, a highly strained interlayer is formed on top of LAO substrate before the growth of S1 phase. This interlayer is fully strained on LAO substrate with *c*/*a* = 1.15 and the formation of misfit dislocations are clearly seen between the interlayer and S1 phase. Figure 2(b) shows a HR-STEM image of S1 phase. Both Bi_2O_2 slab with brighter contrast and Fe–Mn–O slab with darker contrast show zig-zag arrangements. The spacing between the

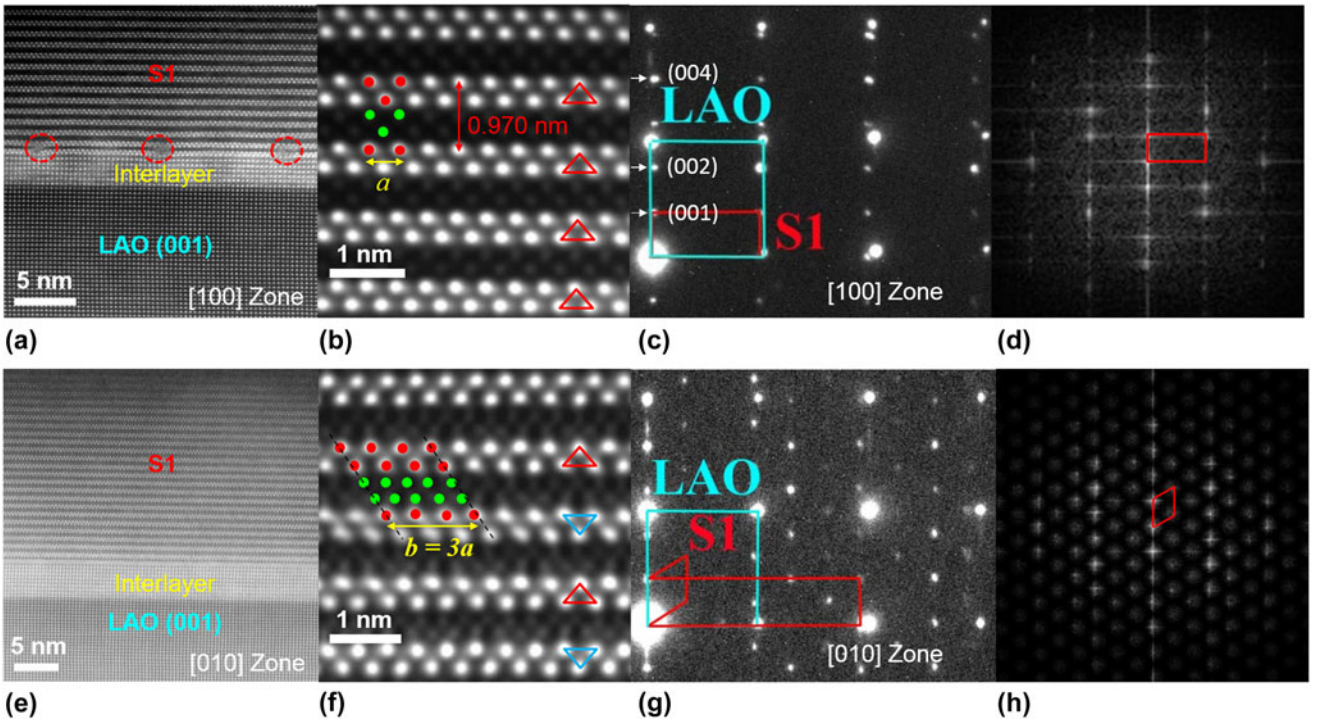


FIG. 2. (a) A cross-sectional STEM overview of S1 phase on LAO substrate in the [100] zone axis with a highly strained interlayer. (b) A representative Cs-corrected HR-STEM image of S1 phase in the [100] zone axis. (c) The corresponding SAED of S1 phase and LAO substrate. (d) The corresponding FFT image. (e) A cross-sectional STEM overview of S1 phase in the [010] zone axis with a highly strained interlayer. (f) A representative Cs-corrected HR-STEM image of S1 phase. (g) The corresponding SAED of S1 phase and LAO substrate in the [010] zone axis. (h) The corresponding FFT image.

https://doi.org/10.1557/jmr.2016.391 Published online by Cambridge University Press

neighboring Bi_2O_2 layer is 9.70 Å, which is twice of the *d*-spacing corresponding to the peak at $2\theta = 18.28°$. The Bi atoms in Bi_2O_2 layer show the same atomic arrangement at the same column, as shown by red triangles in Fig. 2(b). The alternative stacking of Bi_2O_2 and Fe–Mn–O slabs shows a highly epitaxial manner with a commensurate interface. Figure 2(c) shows the SAED pattern for S1 phase in the $[100]_{LAO}$ zone axis. The SAED show that the out-of-plane lattice parameter of S1 is 9.70 Å. Analysis shows that this is half of the *c* lattice parameter of S1 unit cell. The microstructure of S1 phase has also been investigated along $[010]_{LAO}$ zone axis. The highly strained interlayer between S1 phase and LAO substrate is clearly visible. However, no misfit dislocations can be seen along this zone axis [Fig. 2(e)]. As shown in the HR-STEM image in Fig. 2(f), the interface between Fe–Mn–O layer and Bi_2O_2 layer is incommensurated. A detailed discussion on the formation of this new phase can be found elsewhere.[20] The SAED pattern in Fig. 2(g) and FFT image in Fig. 2(h) show a diamond shape with $b = 3a = 11.80$ Å. The SAED patterns in Figs. 2(c)–2(g) are consistent with FFT images in Figs. 2(d)–2(h). Detailed structure of S1 phase has been identified.[52] The BFMO SC structure with S1 phase shows an optical band gap of 3.27 eV and the coexistence of room temperature ferromagnetism and ferroelectricity.[52]

Slightly increasing the growth temperature, pure S2 phase can be obtained, as evidenced by XRD results. Figure 3(a) shows a typical cross-sectional TEM image of S2 phase. An interlayer of ~2 nm was also observed between S2 phase and LAO substrate. It can be seen that S2 phase has layered structure with a spacing of ~12 Å. The SAED pattern shows the out-of-plane lattice parameter is 11.5 Å [Fig. 3(b)]. The microstructure of S2 phase has also been investigated by HR-STEM [Fig. 3(c)]. Different from S1 phase, S2 phase exhibits alternative stacking of single Bi layer and Fe–Mn–O triangle slab. It is reasonable that Bi composition in S2 is less than S1 phase as S2 phase is grown at higher growth temperature and lower laser repetition rate. It should be noted that the diffraction data of S2 phase does not fit any of the well-known BFMO phases. Figure 3(d) shows a zoomed portion of the interface. The highly strained interlayer (with $c/a = 1.28$), is only 3–4 unit cells in thickness. It was reported that tetragonal-like (T-like) $BiFeO_3$ phase grown on LAO and $LaSrAlO_4$ substrates also exhibit

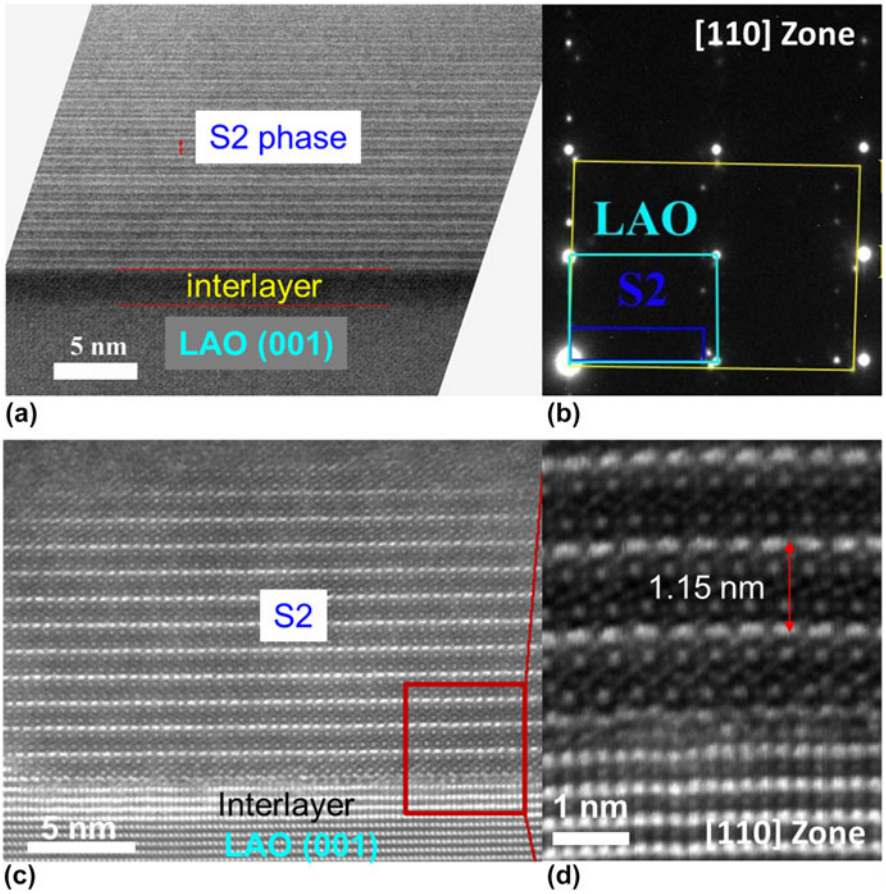


FIG. 3. (a) A cross-sectional TEM overview of the S2 phase on LAO substrate with an interlayer. (b) The corresponding SAED of S2 phase and LAO substrate in the [110] zone axis. (c) A HR-STEM image of S2 phase in the [110] zone axis. (d) The zoomed in HR-STEM image showing the interlayer and S2 phase.

https://doi.org/10.1557/jmr.2016.391 Published online by Cambridge University Press

a huge *c*/*a* ratio (1.2–1.3).[53–55] The T-like $BiFeO_3$ phase with a giant *c*/*a* ratio exhibits enhanced room-temperature multiferroicity.[55] The BFMO interlayer grown on LAO with a high *c*/*a* ratio could be a Mn doped T-like $BiFeO_3$ phase. Both theoretical and experimental explorations on this new material are needed.

It is interesting to note that films directly grown on STO substrates exhibit a conventional tetragonal Bi_2FeMnO_6 with double perovskite structure, as reported previously. The out-of-plane lattice parameter of BFMO is determined to be 3.99 Å. The HAADF-STEM image in Fig. 4(a) shows that the BFMO is completely strained to STO substrate. The *c*/*a* for BFMO on STO is ~1.02. Interestingly, as shown in Fig. 4(b), inserting a thin CeO_2 buffer layer produces a pure supercell structure with the same diffraction peaks as S1. Figure 4(c) shows the formation of this phase on STO substrate with a 25 nm CeO_2 buffer layer. Microstructure analysis shows that this material is the S1 phase grown on LAO substrate [Fig. 4(d)]. The triangle structure of Ce layer provides a template for the growth of S1 phase.[21] It was found that S1 phase has much larger growth window on CeO_2 buffer layer than the direct growth of S1 phase on LAO. The CeO_2 buffer layer provides a broad processing window to grow pure S1 phase. We also found S1 and S2 phases are much resistive than double perovskite BFMO films on STO substrate.

We further explored the film growth by using $BiFeO_3$:$BiCrO_3$ composite targets. Figure 5(a) shows XRD results of films grown at different oxygen pressure, varying from 15 mTorr to 200 mTorr. There are two sets of diffraction peaks. The peaks at 11.53°, 35.06°, 60.28° are defined as X1 phase and peaks at 31.42°, 65.49° are assigned as X2 phase. The out-of-plane lattice parameter is 7.7 Å for X1 phase and 2.84 Å for X2 phase. Mixed phases of X1 and X2 are determined in samples deposited at 15 and 50 mTorr oxygen. Pure X1 phase can be obtained when increasing the oxygen pressure to 200 mTorr. Figure 5(b) shows a typical HRTEM image of X1 phase. The layered structure can be clearly seen. The out-of-plane *d*-spacing is ~7.7 Å, agreeing with XRD results. It is interesting that X1 phase shows

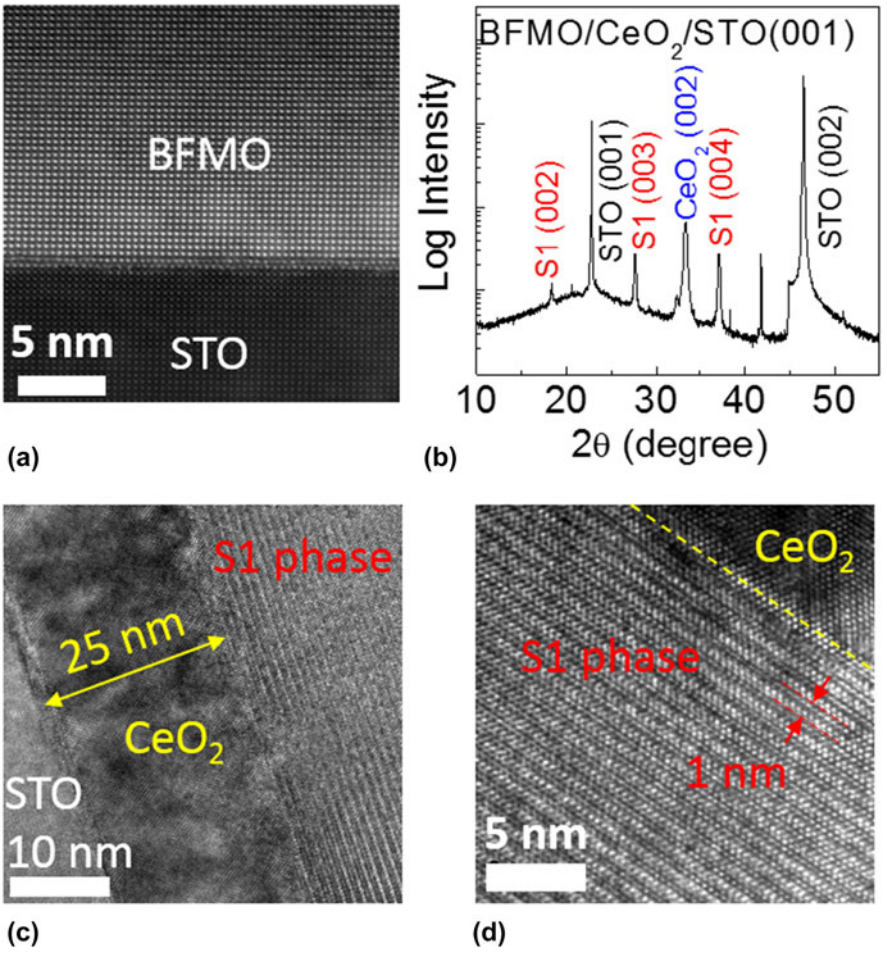


FIG. 4. (a) A typical cross-sectional STEM overview of the tetragonal BFMO phase directly grown on STO. (b) The XRD pattern of S1 phase deposited on CeO_2 buffered STO substrate. (c) A typical cross-sectional TEM overview showing the overview of S1 phase/CeO_2/STO heterostructures. (d) The interface between S1 phase and the CeO_2 buffer layer.

https://doi.org/10.1557/jmr.2016.391 Published online by Cambridge University Press

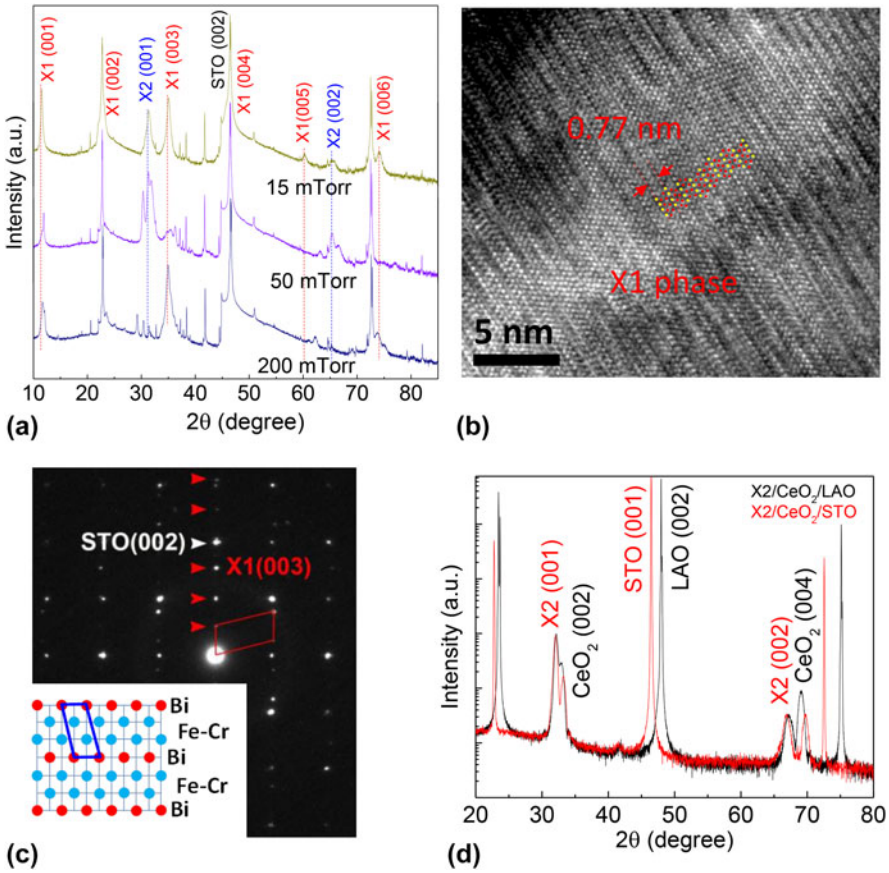


FIG. 5. (a) The XRD pattern of X1 and X2 phases deposited directly on STO substrate at different oxygen pressure. (b) A typical cross-sectional TEM image of X1 phase on STO. (c) The corresponding SAED of X1 phase and STO substrate in the [100] zone axis. The inset shows the atomic arrangement of X1 phase. (d) The XRD pattern of pure X1 phase on CeO_2 buffered STO and LAO substrates.

alternative stacking of Fe–Cr–O triangle slabs and single Bi layer. The diamond diffraction pattern in Fig. 5(c) is stemmed from the neighboring Bi layer, as shown in the inset of Fig. 5(c). The CeO_2 buffer layer has been used to explore the growth of $BiFeO_3$:$BiCrO_3$ composite films. Figure 5(d) shows that pure X2 phase can be obtained on both STO and LAO substrate with a thin CeO_2 buffer layer. It was found that the growth of pure X2 phase can be obtained in different oxygen pressure, indicating CeO_2 buffer layer broadens the growth window for this phase. The triangle template in CeO_2 buffer layer can also be the reason for the growth of this X2 phase, similar to the phenomena of S1 phase on CeO_2 buffer layer. This result indicates that different materials with potential multiferroicity can be grown by using a composite target composed of two perovskite bismuth compounds. In addition, CeO_2 buffer layer can be used as a general template for the growth of materials in $BiRO_3$ (R = Cr, Mn, Fe, Co, Ni). Identifying the detailed crystal structure and compositions of these new materials will be critical for their applications and further studies.

IV. CONCLUSION

We explored the thin films with unexpected phases grown using composite $BiFeO_3$:$BiMnO_3$ and $BiFeO_3$:$BiCrO_3$ targets. Bi_2FeMnO_6 tetragonal phase can often be grown directly on STO substrates, while other phases can be obtained on LAO substrates. A thin layer of CeO_2 buffer layer promotes the growth of S1 phase and broadens the growth window for such a phase. The growth of new materials has also been studied using a $BiFeO_3$:$BiCrO_3$ target. The X1 and X2 phases have been grown on STO substrates. Pure X2 phase can be obtained on CeO_2 buffered STO and LAO substrates. This work not only demonstrates that unexpected materials can be synthesized by using a composite perovskite $BiRO_3$ (R = Cr, Mn, Fe, Co, Ni) target, but also demonstrate that CeO_2 buffer layer can serve as a template for the growth of these materials.

ACKNOWLEDGMENTS

The work at Los Alamos National Laboratory was supported by the NNSA's Laboratory Directed Research

https://doi.org/10.1557/jmr.2016.391 Published online by Cambridge University Press

and Development Program and was performed, in part, at the Center for Integrated Nanotechnologies, an Office of Science User Facility operated for the U.S. Department of Energy (DOE) Office of Science. Los Alamos National Laboratory, an affirmative action equal opportunity employer, is operated by Los Alamos National Security, LLC, for the National Nuclear Security Administration of the U.S. Department of Energy under contract DE-AC52-06NA25396. The work at Texas A&M and Purdue University is funded by the Office of Naval Research N00014-15-1-2362 (Texas A&M) and N00014-16-1-2465 (Purdue). The TEM work is funded by the U.S. National Science Foundation (DMR-1565822).

REFERENCES

1. J. Narayan, N. Biunno, R. Singh, O.W. Holland, and O. Auciello: Formation of thin superconducting films by the laser processing method. *Appl. Phys. Lett.* **51**, 1845 (1987).
2. J. Allibe, I.C. Infante, S. Fusil, K. Bouzehouane, E. Jacquet, C. Deranlot, M. Bibes, and A. Barthelemy: Coengineering of ferroelectric and exchange bias properties in $BiFeO_3$ based heterostructures. *Appl. Phys. Lett.* **95**, 182503 (2009).
3. A.P. Chen, F. Khatkhatay, W. Zhang, C. Jacob, L. Jiao, and H.Y. Wang: Strong oxygen pressure dependence of ferroelectricity in $BaTiO_3/SrRuO_3/SrTiO_3$ epitaxial heterostructures. *J. Appl. Phys.* **114**, 124101 (2013).
4. Q. Su, S.M. Cho, Z.X. Bi, A.P. Chen, and H.Y. Wang: Enhanced electrochemical properties of Bi-layer $La_{0.5}Sr_{0.5}CoO_{3\text{-delta}}$ cathode prepared by a hybrid method. *Electrochim. Acta* **56**, 3969 (2011).
5. Z. Li, L. You, Z. Yang, H.R. Tan, P. Ren, X.F. Chen, J.S. Pan, J.L. Wang, L. Wang, M. Bosman, W.G. Zhu, and Z.L. Dong: Multiferroicity in manganite/titanate superlattices determined by oxygen pressure-mediated cation defects. *J. Appl. Phys.* **113**, 164302 (2013).
6. S. Singh, J. Xiong, A.P. Chen, M.R. Fitzsimmons, and Q.X. Jia: Field-dependent magnetization of $BiFeO_3$ in an ultrathin $La_{0.7}Sr_{0.3}MnO_3/BiFeO_3$ superlattice. *Phys. Rev. B: Condens. Matter Mater. Phys.* **92**, 224405 (2015).
7. A.K. Yadav, C.T. Nelson, S.L. Hsu, Z. Hong, J.D. Clarkson, C.M. Schlepuetz, A.R. Damodaran, P. Shafer, E. Arenholz, L.R. Dedon, D. Chen, A. Vishwanath, A.M. Minor, L.Q. Chen, J.F. Scott, L.W. Martin, and R. Ramesh: Observation of polar vortices in oxide superlattices. *Nature* **530**, 198 (2016).
8. A.P. Chen, Z.X. Bi, C.F. Tsai, J. Lee, Q. Su, X.H. Zhang, Q.X. Jia, J.L. MacManus-Driscoll, and H.Y. Wang: Tunable low-field magnetoresistance in $(La_{0.7}Sr_{0.3}MnO_3)_{0.5}:(ZnO)_{0.5}$ self-assembled vertically aligned nanocomposite thin films. *Adv. Funct. Mater.* **21**, 2423 (2011).
9. F. Khatkhatay, A.P. Chen, J.H. Lee, W.R. Zhang, H. Abdel-Raziq, and H.Y. Wang: Ferroelectric properties of vertically aligned nanostructured $BaTiO_3$–CeO_2 thin films and their integration on silicon. *ACS Appl. Mater. Interfaces* **5**, 12541 (2013).
10. W.R. Zhang, A.P. Chen, J. Jian, Y.Y. Zhu, L. Chen, P. Lu, Q.X. Jia, J.L. MacManus-Driscoll, X.H. Zhang, and H.Y. Wang: Strong perpendicular exchange bias in epitaxial $La_{0.7}Sr_{0.3}MnO_3$: $BiFeO_3$ nanocomposite films through vertical interfacial coupling. *Nanoscale* **7**, 13808 (2015).
11. N. Aimon, H.K. Choi, X.Y. Sun, D.H. Kim, and C.A. Ross: Templated self-assembly of functional oxide nanocomposites. *Adv. Mater.* **26**, 3063 (2014).
12. S.M. Stratulat, X.L. Lu, A. Morelli, D. Hesse, W. Erfurth, and M. Alexe: Nucleation-induced self-assembly of multiferroic $BiFeO_3$–$CoFe_2O_4$ nanocomposites. *Nano Lett.* **13**, 3884 (2013).
13. H.M. Zheng, F. Straub, Q. Zhan, P.L. Yang, W.K. Hsieh, F. Zavaliche, Y.H. Chu, U. Dahmen, and R. Ramesh: Self-assembled growth of $BiFeO_3$–$CoFe_2O_4$ nanostructures. *Adv. Mater.* **18**, 2747 (2006).
14. H.J. Liu, V.T. Tra, Y.J. Chen, R. Huang, C.G. Duan, Y.H. Hsieh, H.J. Lin, J.Y. Lin, C.T. Chen, Y. Ikuhara, and Y.H. Chu: Large magnetoresistance in magnetically coupled $SrRuO_3$–$CoFe_2O_4$ self-assembled nanostructures. *Adv. Mater.* **25**, 4753 (2013).
15. W.R. Zhang, L.G. Li, P. Lu, M. Fan, Q. Su, F. Khatkhatay, A.P. Chen, Q.X. Jia, X.H. Zhang, J.L. MacManus-Driscoll, and H.Y. Wang: Perpendicular exchange-biased magnetotransport at the vertical heterointerfaces in $La_{0.7}Sr_{0.3}MnO_3$:NiO nanocomposites. *ACS Appl. Mater. Interfaces* **7**, 21646 (2015).
16. W.R. Zhang, A.P. Chen, Z.K. Bi, Q.X. Jia, J.L. MacManus-Driscoll, and H.Y. Wang: Interfacial coupling in heteroepitaxial vertically aligned nanocomposite thin films: From lateral to vertical control. *Curr. Opin. Solid State Mater. Sci.* **18**, 6 (2014).
17. A.P. Chen, J-M. Hu, P. Lu, T.N. Yang, W. Zhang, L. Li, T. Ahmed, E. Enriquez, M. Weigand, Q. Su, H.Y. Wang, J-X. Zhu, J.L. MacManus-Driscoll, L.Q. Chen, D. Yarotski, and Q.X. Jia: Role of scaffold network in controlling strain and functionalities of nanocomposite films. *Sci. Adv.* **2**, e1600245 (2016).
18. J.L. MacManus-Driscoll: Self-assembled heteroepitaxial oxide nanocomposite thin film structures: Designing interface-induced functionality in electronic materials. *Adv. Funct. Mater.* **20**, 2035 (2010).
19. A.P. Chen, H.H. Zhou, Z.X. Bi, Y.Y. Zhu, Z.P. Luo, A. Bayraktaroglu, J. Phillips, E.M. Choi, J.L. MacManus-Driscoll, S.J. Pennycook, J. Narayan, Q.X. Jia, X.H. Zhang, and H.Y. Wang: A new class of room-temperature multiferroic thin films with bismuth-based supercell structure. *Adv. Mater.* **25**, 1028 (2013).
20. Y.Y. Zhu, A.P. Chen, H.H. Zhou, W.R. Zhang, J. Narayan, J.L. MacManus-Driscoll, Q.X. Jia, and H.Y. Wang: Research Updates: Epitaxial strain relaxation and associated interfacial reconstructions: The driving force for creating new structures with integrated functionality. *APL Mater.* **1**, 050702 (2013).
21. L.G. Li, W.R. Zhang, F. Khatkhatay, J. Jian, M. Fan, Q. Su, Y.Y. Zhu, A.P. Chen, P. Lu, X.H. Zhang, and H.Y. Wang: Strain and interface effects in a novel Bismuth-based self-assembled supercell structure. *ACS Appl. Mater. Interfaces* **7**, 11631 (2015).
22. E.M. Choi, S. Patnaik, E. Weal, S.L. Sahonta, H. Wang, Z. Bi, J. Xiong, M.G. Blamire, Q.X. Jia, and J.L. MacManus-Driscoll: Strong room temperature magnetism in highly resistive strained thin films of $BiFe_{0.5}Mn_{0.5}O_3$. *Appl. Phys. Lett.* **98**, 012509 (2011).
23. J. Miao, X. Zhang, Q. Zhan, Y. Jiang, and K.H. Chew: Bi-relaxation behaviors in epitaxial multiferroic double-perovskite $BiFe_{0.5}Mn_{0.5}O_3/CaRuO_3$ heterostructures. *Appl. Phys. Lett.* **99**, 062905 (2011).
24. P. Liu, Z.X. Cheng, Y. Du, L.Y. Feng, H. Fang, X.L. Wang, and S.X. Dou: Anisotropy of crystal growth mechanisms, dielectricity, and magnetism of multiferroic Bi_2FeMnO_6 thin films. *J. Appl. Phys.* **113**, 17D904 (2013).
25. L. Bi, A.R. Taussig, H.S. Kim, L. Wang, G.F. Dionne, D. Bono, K. Persson, G. Ceder, and C.A. Ross: Structural, magnetic, and optical properties of $BiFeO_3$ and Bi_2FeMnO_6 epitaxial thin films: An experimental and first-principles study. *Phys. Rev. B: Condens. Matter Mater. Phys.* **78**, 104106 (2008).

https://doi.org/10.1557/jmr.2016.391 Published online by Cambridge University Press

26. H.Y. Zhao, H. Kimura, Z.X. Cheng, X.L. Wang, and T. Nishida: Room temperature multiferroic properties of Nd:$BiFeO_3$/Bi_2FeMnO_6 bilayered films. *Appl. Phys. Lett.* **95**, 232904 (2009).
27. E.M. Choi, T. Fix, A. Kursumovic, C.J. Kinane, D. Arena, S.L. Sahonta, Z.X. Bi, J. Xiong, L. Yan, J.S. Lee, H.Y. Wang, S. Langridge, Y.M. Kim, A.Y. Borisevich, I. MacLaren, Q.M. Ramasse, M.G. Blamire, Q.X. Jia, and J.L. MacManus-Driscoll: Room temperature ferrimagnetism and ferroelectricity in strained, thin films of $BiFe_{0.5}Mn_{0.5}O_3$. *Adv. Funct. Mater.* **24**, 7478 (2014).
28. E.M. Choi, J.E. Kleibeuker, T. Fix, J. Xiong, C.J. Kinane, D. Arena, S. Langridge, A.P. Chen, Z.X. Bi, J.H. Lee, H.Y. Wang, Q.X. Jia, M.G. Blamire, and J.L. MacManus-Driscoll: Interface-Coupled $BiFeO_3$/$BiMnO_3$ superlattices with magnetic transition temperature up to 410 K. *Adv. Mater. Interfaces* **3**, 1500597 (2016).
29. M. Azuma, K. Takata, T. Saito, S. Ishiwata, Y. Shimakawa, and M. Takano: Designed ferromagnetic, ferroelectric Bi_2NiMnO_6. *J. Am. Chem. Soc.* **127**, 8889 (2005).
30. R. Nechache, L.P. Carignan, L. Gunawan, C. Harnagea, G.A. Botton, D. Menard, and A. Pignolet: Epitaxial thin films of multiferroic Bi_2FeCrO_6 with B-site cationic order. *J. Mater. Res.* **22**, 2102 (2007).
31. R. Nechache, C. Harnagea, L.P. Carignan, O. Gautreau, L. Pintilie, M.P. Singh, D. Menard, P. Fournier, M. Alexe, and A. Pignolet: Epitaxial thin films of the multiferroic double perovskite Bi_2FeCrO_6 grown on (100)-oriented $SrTiO_3$ substrates: Growth, characterization, and optimization. *J. Appl. Phys.* **105**, 061621 (2009).
32. S. Li, B. AlOtaibi, W. Huang, Z.T. Mi, N. Serpone, R. Nechache, and F. Rosei: Epitaxial Bi_2FeCrO_6 multiferroic thin film as a new visible light absorbing photocathode material. *Small* **11**, 4018 (2015).
33. A. Lotnyk, S. Senz, and D. Hesse: Epitaxial growth of TiO_2 thin films on $SrTiO_3$, $LaAlO_3$ and yttria-stabilized zirconia substrates by electron beam evaporation. *Thin Solid Films* **515**, 3439 (2007).
34. B.H. Park, J.Y. Huang, L.S. Li, and Q.X. Jia: Role of atomic arrangements at interfaces on the phase control of epitaxial TiO_2 films. *Appl. Phys. Lett.* **80**, 1174 (2002).
35. A.P. Chen, Z.X. Bi, W.R. Zhang, J. Jian, Q.X. Jia, and H.Y. Wang: Textured metastable VO_2 (B) thin films on $SrTiO_3$ substrates with significantly enhanced conductivity. *Appl. Phys. Lett.* **104**, 071909 (2014).
36. J. Jian, A.P. Chen, W.R. Zhang, and H.Y. Wang: Sharp semiconductor-to-metal transition of VO_2 thin films on glass substrates. *J. Appl. Phys.* **114**, 244301 (2013).
37. T.H. Yang, R. Aggarwal, A. Gupta, H.H. Zhou, R.J. Narayan, and J. Narayan: Semiconductor-metal transition characteristics of VO_2 thin films grown on c- and r-sapphire substrates. *J. Appl. Phys.* **107**, 053514 (2010).
38. A. Gupta, R. Aggarwal, P. Gupta, T. Dutta, R.J. Narayan, and J. Narayan: Semiconductor to metal transition characteristics of VO_2 thin films grown epitaxially on Si(001). *Appl. Phys. Lett.* **95**, 111915 (2009).
39. A.P. Chen, H. Long, X.C. Li, Y.H. Li, G. Yang, and P.X. Lu: Controlled growth and characteristics of single-phase Cu_2O and CuO films by pulsed laser deposition. *Vacuum* **83**, 927 (2009).
40. M. Golalikhani, Q.Y. Lei, G. Chen, J.E. Spanier, H. Ghassemi, C.L. Johnson, M.L. Taheri, and X.X. Xi: Stoichiometry of $LaAlO_3$ films grown on $SrTiO_3$ by pulsed laser deposition. *J. Appl. Phys.* **114**, 027008 (2013).
41. G.Z. Liu, Q.Y. Lei, and X.X. Xi: Stoichiometry of $SrTiO_3$ films grown by pulsed laser deposition. *Appl. Phys. Lett.* **100**, 202902 (2012).
42. L. You, N.T. Chua, K. Yao, L. Chen, and J.L. Wang: Influence of oxygen pressure on the ferroelectric properties of epitaxial $BiFeO_3$ thin films by pulsed laser deposition. *Phys. Rev. B: Condens. Matter Mater. Phys.* **80**, 024105 (2009).
43. M.P. Warusawithana, C. Richter, J.A. Mundy, P. Roy, J. Ludwig, S. Paetel, T. Heeg, A.A. Pawlicki, L.F. Kourkoutis, M. Zheng, M. Lee, B. Mulcahy, W. Zander, Y. Zhu, J. Schubert, J.N. Eckstein, D.A. Muller, C.S. Hellberg, J. Mannhart, and D.G. Schlom: $LaAlO_3$ stoichiometry is key to electron liquid formation at $LaAlO_3$/$SrTiO_3$ interfaces. *Nat. Commun.* **4**, 2351 (2013).
44. H. Long, G. Yang, A.P. Chen, Y.H. Li, and P.X. Lu: Growth and characteristics of laser deposited anatase and rutile TiO_2 films on Si substrates. *Thin Solid Films* **517**, 745 (2008).
45. A. Srivastava, H. Rotella, S. Saha, B. Pal, G. Kalon, S. Mathew, M. Motapothula, M. Dykas, P. Yang, E. Okunishi, D.D. Sarma, and T. Venkatesan: Selective growth of single phase VO_2(A, B, and M) polymorph thin films. *APL Mater.* **3**, 026101 (2015).
46. H. Bea, M. Bibes, A. Barthelemy, K. Bouzehouane, E. Jacquet, A. Khodan, J.P. Contour, S. Fusil, F. Wyczisk, A. Forget, D. Lebeugle, D. Colson, and M. Viret: Influence of parasitic phases on the properties of $BiFeO_3$ epitaxial thin films. *Appl. Phys. Lett.* **87**, 072508 (2005).
47. X.J. Lu, J.W. Howard, A.P. Chen, J.L. Zhu, S. Li, G. Wu, P. Dowden, H.W. Xu, Y.S. Zhao, and Q.X. Jia: Antiperovskite Li_3OCl superionic conductor films for solid-state Li-ion batteries. *Adv. Sci.* **3**, 1500359 (2016).
48. A.P. Chen, Z.X. Bi, Q.X. Jia, J.L. MacManus-Driscoll, and H.Y. Wang: Microstructure, vertical strain control and tunable functionalities in self-assembled, vertically aligned nanocomposite thin films. *Acta Mater.* **61**, 2783 (2013).
49. D.S. Kan and Y. Shimakawa: Controlled cation stoichiometry in pulsed laser deposition-grown $BaTiO_3$ epitaxial thin films with laser fluence. *Appl. Phys. Lett.* **99**, 081907 (2011).
50. S. Kobayashi, Y. Tokuda, T. Ohnishi, T. Mizoguchi, N. Shibata, Y. Sato, Y. Ikuhara, and T. Yamamoto: Cation off-stoichiometric $SrMnO_{3\text{-}delta}$ thin film grown by pulsed laser deposition. *J. Mater. Sci.* **46**, 4354 (2011).
51. P.C. Dowden, Z. Bi, and Q.X. Jia: Method for controlling energy density for reliable pulsed laser deposition of thin films. *Rev. Sci. Instrum.* **85**, 025111 (2014).
52. W.R. Zhang, M.T. Li, A.P. Chen, L.G. Li, Y.Y. Zhu, Z.H. Xia, P. Lu, P. Boullay, L.J. Wu, Y.M. Zhu, J.L. MacManus-Driscoll, Q.X. Jia, H.H. Zhou, J. Narayan, X.H. Zhang, and H.Y. Wang: Two-dimensional layered oxide structures tailored by self assembled layer stacking via interfacial strain. *ACS Appl. Mater. Interfaces* **8**, 16845 (2016).
53. Z.H. Chen, Z.L. Luo, C.W. Huang, Y.J. Qi, P. Yang, L. You, C.S. Hu, T. Wu, J.L. Wang, C. Gao, T. Sritharan, and L. Chen: Low-symmetry monoclinic phases and polarization rotation path mediated by epitaxial strain in multiferroic $BiFeO_3$ thin films. *Adv. Funct. Mater.* **21**, 133 (2011).
54. D. Mazumdar, V. Shelke, M. Iliev, S. Jesse, A. Kumar, S.V. Kalinin, A.P. Baddorf, and A. Gupta: Nanoscale switching characteristics of nearly tetragonal $BiFeO_3$ thin films. *Nano Lett.* **10**, 2555 (2010).
55. H. Bea, B. Dupe, S. Fusil, R. Mattana, E. Jacquet, B. Warot-Fonrose, F. Wilhelm, A. Rogalev, S. Petit, V. Cros, A. Anane, F. Petroff, K. Bouzehouane, G. Geneste, B. Dkhil, S. Lisenkov, I. Ponomareva, L. Bellaiche, M. Bibes, and A. Barthelemy: Evidence for room-temperature multiferroicity in a compound with a giant axial ratio. *Phys. Rev. Lett.* **102**, 217603 (2009).

https://doi.org/10.1557/jmr.2016.391 Published online by Cambridge University Press